This is a preprint of the following article, which is available at: http://mdolab.engin.umich.edu
B. J. Brelje and J. R. R. A. Martins. Aerostructural wing optimization for a hydrogen fuel cell aircraft. *AIAA SCITECH*, January 2021.
The original article may differ from this preprint and is available at https://arc.aiaa.org/doi/abs/10.2514/6.2021-1132.

Aerostructural Wing Optimization for a Hydrogen Fuel Cell Aircraft

Benjamin J. Brelje* and Joaquim R. R. A. Martins †
University of Michigan Department of Aerospace Engineering, Ann Arbor, MI 48109

Hydrogen has been identified as a potential fuel for air transportation without carbon emissions. Hydrogen contains much higher energy per unit mass than any conceivable rechargeable battery, potentially making longer-range missions possible than pure electric configurations. However, hydrogen's low volumetric energy density presents practical challenges. Hydrogen must either be kept under deep cryogenic conditions or compressed under very high pressure. Either solution is likely to require adding significant drag and tank weight to the airplane. This is a packing optimization problem subject to aerostructural physics, and we can employ multidisciplinary design optimization techniques to provide insight into optimal wing design for novel hydrogen aircraft concepts. In this paper, we extend prior work on wing packing optimization subject to aerodynamics only, and now incorporate structural analysis and structure geometry into the problem. We optimize the range of a hydrogen-electric aircraft with hydrogen fuel storage located inside the wing outer mold line. The geometry of the hydrogen storage tanks influences the shape of the wing as well as the weight and volumetric capacity of the tank. While the effect of hydrogen storage on other aircraft concepts cannot be generalized from this study, the optimization methods we use are promising for performing relevant aircraft design trade studies. The optimizer finds the correct tradeoff between weight, drag, and fuel storage for the mission, subject to spatial integration feasibility. In our test scenario, we find that the optimal aerostructural design involves substantial wing root thickening.

I. Introduction

Electric propulsion is rapidly evolving as a research topic where one of the most pressing technical challenges is increasing range capability [1]. The limited specific energy of today's batteries (on the order of 200 $\mathrm{Wh\,kg^{-1}}$) [1] places unacceptable limits on design range for important applications, such as single-aisle commercial air transport. Hybrid-electric designs can exploit electric motors to reduce weight, fuel burn, cost, and drag [1], but they still consume fuel and remain a point source of carbon dioxide (CO_2) emissions.

Hydrogen fuel can theoretically alleviate the range issues of battery-electric propulsion without producing point-source CO_2 emissions. Fuel cells consume hydrogen and produce electricity, emitting only water vapor [2]. Alternatively, hydrogen can be burned in adapted engines, emitting water vapor and trace nitrogen oxides [3]. If the hydrogen is produced cleanly (e.g., through electrolysis powered by renewable energy), it can achieve CO_2-free flying. While the impact (and potential mitigation) of high-altitude water vapor emissions on climate change is not entirely clear, eliminating CO_2 emissions would be a significant step towards greener aviation.

Hydrogen fuel in aviation has a surprisingly long history. Soon after liquid hydrogen was first produced for the space program, NACA experimented with hydrogen combustion aircraft concepts. Silverstein and Hall [4] proposed using hydrogen fuel for a subsonic high-altitude bomber (Figure 1) in a declassified 1955 NACA research memo. Even then, it was apparent that integrating the enormous hydrogen tanks into the aircraft would be a significant challenge. From 1957 to 1959, NACA flew a B-57 Canberra bomber (Figure 2) converted to run one engine using liquid hydrogen

*PhD Candidate, AIAA Student Member
†Professor, AIAA Fellow

fuel [5]. The airplane was able to transition from jet fuel to hydrogen and back again on numerous successful flights. The pilots noted that the hydrogen-powered engine tended to leave contrails even when the kerosene-powered engine did not. Simultaneously, Kelly Johnson's Skunk Works was seriously considering building a hydrogen-powered supersonic bomber [5]. The study airplane, known as the CL-400 Suntan, was canceled by 1958, but the government learned valuable insights on the safe handling of hydrogen fuels.

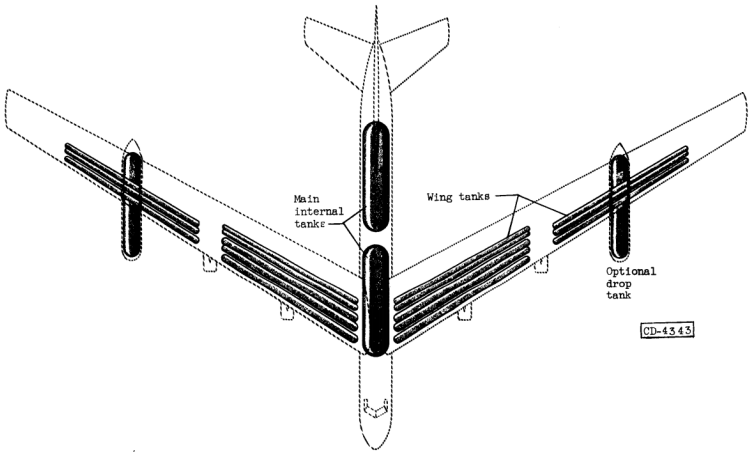

Fig. 1 The Silverstein–Hall subsonic bomber concept used liquid hydrogen tanks in both the wing and fuselage [4]

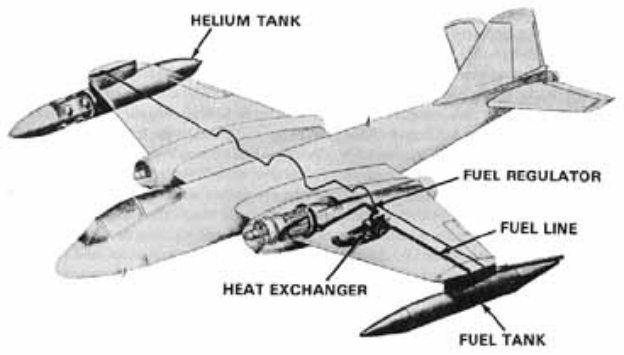

Fig. 2 NACA's converted B-57 testbed used liquid hydrogen to power one engine [5]

After the cancellation of the CL-400, hydrogen aviation fuel was not seriously pursued operationally again. However, the concept is experiencing a renaissance. In the last two decades, prototype hydrogen-powered aircraft have been built and flown, including the Hy4 [6] and Boeing Fuel Cell Demonstrator [2]. NASA has also funded a university consortium to examine liquid hydrogen propulsion for transport aircraft applications [3]. Finally, the concept seems to be gaining some traction in industry, with both startups (ZeroAvia) and incumbents (Airbus) promoting hydrogen as environmentally-friendly alternatives to petroleum fuels [3].

Notwithstanding hydrogen's very high energy mass density, its volumetric density under normal conditions is much lower than jet fuel [3]. Commercial aircraft carry the vast majority of their fuel in sealed wing tanks without significant aerodynamic penalty; hydrogen at ambient pressure is volume-limited in the same space. Therefore, while hydrogen alleviates some of the weight challenges of green aviation concepts, it creates a new *spatial integration* challenge. Spatial integration involves the packing of all required passengers, payload, structural elements, fuel, and equipment into a feasible aircraft layout [7].

In this paper, we introduce an optimization-based method for integrating compressed hydrogen fuel into a wing with minimum weight and drag penalty. This is not a hydrogen aircraft design study *per se*. Instead, we introduce a new

methodology and validate that it performs well on a relevant wing design test case. We do not claim to have designed a feasible or desirable airplane at the top level (e.g., we do not consider fuselage design or propulsion). We also do not claim that design trends observed on this test case are generalizable to other potential hydrogen aircraft configurations.

II. Packing Optimization in Multidisciplinary Design Optimization

Packing optimization problems are well known in the operations research literature, but the formulations developed for other canonical problems (reviewed by Brelje et al. [7]) are not well suited to gradient-based optimization. On the other hand, the differentiable geometry constraints commonly used in gradient-based shape optimization (such as one- and two-dimensional thicknesses; also reviewed by Brelje et al. [7]) are not flexible or general enough to handle arbitrary packing problems. To overcome these limitations, Brelje et al. [7] formulated a more general packing constraint based on the Kreisselmeier–Steinhauser (KS) aggregation function. The KS constraint formulation is smooth and differentiable, making it useful for gradient-based multidisciplinary design optimization (MDO).

Subsequently, we applied this methodology to design minimum-drag aeroshells around a human avatar [7] and the maximum-range wing-battery combination for a notional electric aircraft [8]. For the latter problem, batteries inside the wing box were optimized together with the outer mold line for maximum Breguet range $V_{\text{battery}} L/D$ subject to aerodynamic analysis only. We found that the optimizer found the correct tradeoff between wing thinness (advantageous for drag) versus thickness (beneficial for energy storage). We also found that sectioning the battery into three banks substantially increased the packing efficiency of the battery and extended aircraft range. However, neither of the previous examples involved multidisciplinary physics (e.g., aerodynamic and structural design), and the complexity of the packing problem was simple compared to problems of broader industrial interest. A packing problem with both high-fidelity multidisciplinary physics and many objects to pack has not yet been demonstrated.

III. Problem Description

This work extends the wing packing design optimization problem described by Brelje and Martins [8] to the aerostructural domain. Considering structure complicates the wing packing optimization problem in three primary ways. First, the structural analysis enables the airplane model to vary both weight and drag, likely producing a different optimal design than when considering aerodynamics alone. Second, structural members such as spars and ribs significantly increase the packing problem's complexity compared to considering the wing OML only. Finally, each optimization iteration's computational cost significantly increases because an iterative solution to the aerostructural problem is now required, and a coupled-adjoint must also be computed.

A. Wing Description

The baseline wing design is representative of a simple, single-aisle transport aircraft and is identical to the wing featured in the University of Michigan MDO Lab aerodynamic shape optimization tutorial*. The wing planform is modeled after the Douglas DC-9, but we use a RAE2822 transonic airfoil at baseline. The wingbox front and rear spar locations generally approximate the proportions of the DC-9 wing structure (Figure 3). We generated a conventional wingbox structural layout with 18 evenly-spaced rib bays and 8 stringers between the spars. The stringers each run all the way out to the end of the wing box. The cruise condition is Mach 0.8 at 10,000 m altitude. The baseline weight at cruise is 54,900 kg, which equates to approximately $C_L = 0.5$. We compute structural loads at a 2.5 g static condition, flown at Mach 0.75 and 5,000 m altitude.

B. Tank Description

Unlike the previous wing problem that featured a battery, we optimize a set of seven hydrogen tanks in each wing root (one per rib bay). The 700 bar compressed hydrogen tanks are cylindrical with spherical endcaps. Each tank can vary in radius and length, with additional variables to position each tank relative to its rib bay (Figure 4). The tanks consist of optimized carbon fiber reinforced polymer (CFRP) laminate.

*https://github.com/mdolab/mach-aero

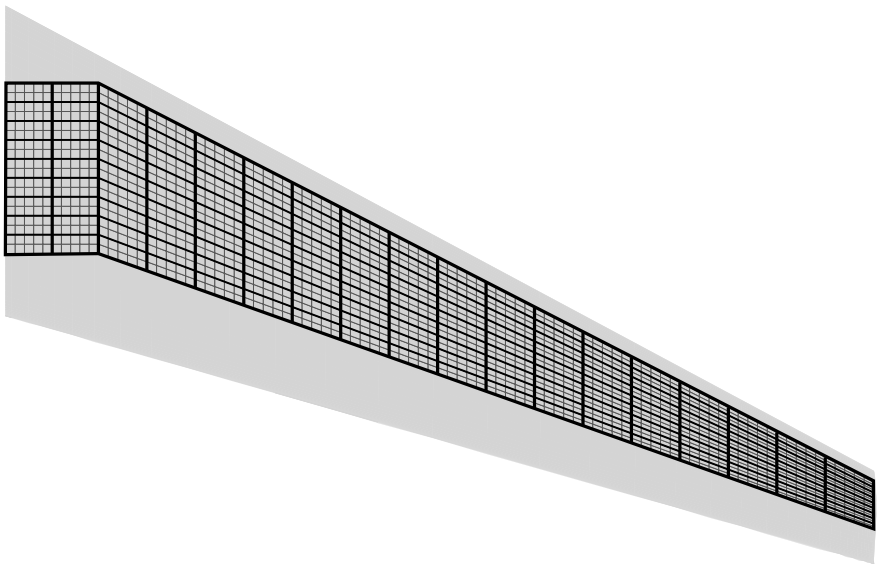

Fig. 3 Wingbox structural mesh overlaid on OML planform

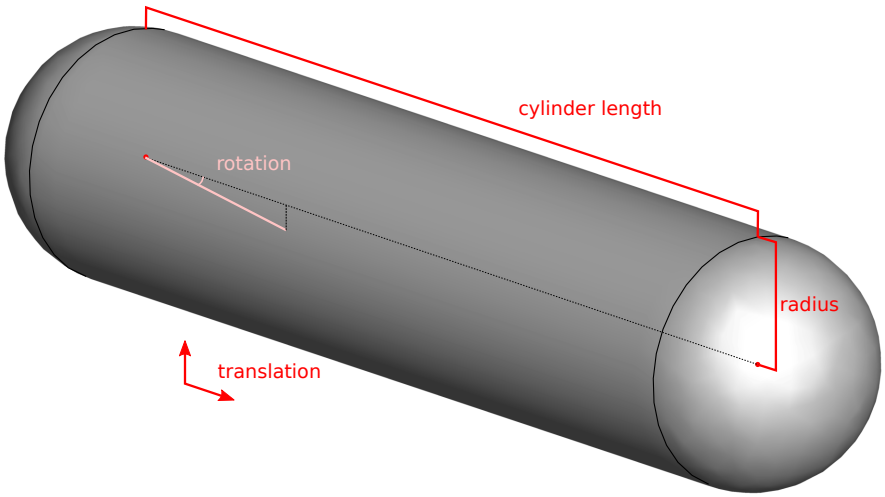

Fig. 4 A representative compressed hydrogen tank with design variables labeled

IV. Methodology

To perform aerostructural analysis and design, we used the MDO of Aircraft Configurations with High Fidelity (MACH) framework [9]. The MACH framework integrates several high-fidelity analysis tools with geometry engines while propagating design variable derivatives [10]. The subset of aerodynamic shape optimization tools is open-source and freely available.

A. Aerostructural Analysis

We used the open-source ADflow solver for aerodynamic analysis and derivatives [11]. ADflow is a structured, multiblock, overset RANS solver with discrete adjoint gradients. We use the Spalart–Allmaras turbulence model and an approximate Newton–Krylov solver for this problem [12]. The aerodynamic mesh (Figure 5) consists of approximately 800,000 volume cells and was generated using pyHyp [13], an open-source implementation of the hyperbolic scheme described in [14]. The aero solver settings and mesh are virtually identical to those in the MACH aero shape optimization

tutorial[†].

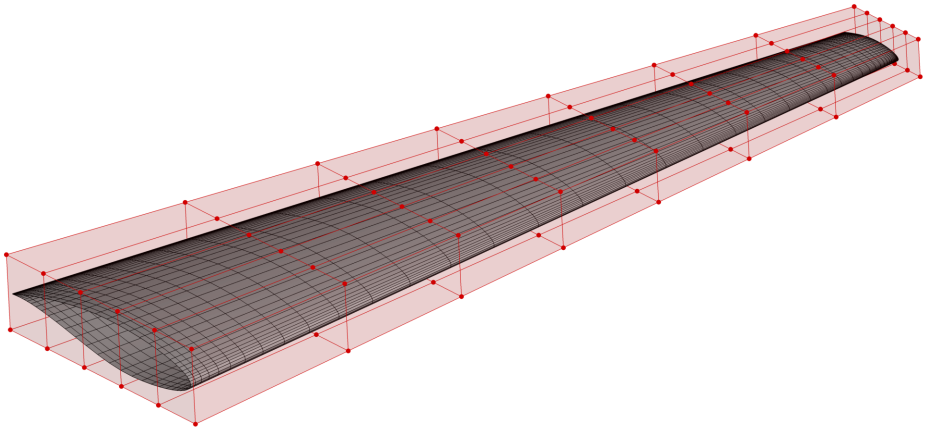

Fig. 5 Aerodynamic surface mesh pictured with free-form deformation (FFD) control points

For structural analysis, we use the open-source finite element solver TACS [15]. TACS computes efficient adjoint derivatives with respect to the structural sizing (thickness) variables and geometry. The structural mesh consists of 7,632 CQUAD4 elements (Figure 3), with explicitly-modeled stringers. We only performed a linear static analysis in this scenario, though TACS supports geometric nonlinearity and buckling.

Because structural deflections affect the aerodynamic surface and vice-versa, an aerostructural solver is required. We use a block Gauss–Seidel approach to solve the aerostructural analysis and a Krylov method to solve the coupled adjoint [10].

B. Geometry

We use two different geometry engines in this problem; one for the wing and one for the hydrogen tanks. The wing was parameterized using the free-form deformation (FFD) method [16] using the open-source implementation in pyGeo [17]. The FFD volume (Figure 5) is identical to the one generated in the MACH aero tutorial and contains 96 design variables. Both the CFD surface mesh coordinates and the structural elements are embedded in the same FFD volume, so geometric displacements are always consistent between the two. CFD surface mesh displacements are propagated to the volume using IDwarp, an open-source implementation of the inverse-distance weighted warping scheme from [18].

We use a different approach to parameterize the tank geometry. An initial triangulated representation of each tank surface is generated using Engineering Sketch Pad (ESP) [19], an open-source CAD application. Using a Python wrapper around ESP's OpenCSM library, we map each point on the tank surface onto the CAD B-spline surface in parametric coordinates and save the result. When the geometry is perturbed, we retrieve a new set of surface mesh points using the same parametric coordinates. This way, the topology of the mesh is preserved across geometric perturbations. The design variables are as pictured in Figure 4—five variables per tank, for a total of 35.

Gradients with respect to geometric design variables are computed using a parallel finite differencing approach. Since the aerostructural design optimization is done in a high-performance computing (HPC) environment with 100 or more available cores, we can perform finite differences across dozens of geometry variables without incurring much cost in terms of wall time (a few seconds). The advantages of using this open-source CAD package were readily apparent at several points. For example, we were able to edit the source to suppress certain console output, which, while useful in interactive mode, clogs the output when running dozens of instances simultaneously. Open source code also made the Python wrapper possible, which was indispensable for this project.

The spatial integration constraints are computed using a newly-developed software package, geograd. Geograd is a reimplementation of the method described by Brelje et al. [7] in Fortran. The software computes two metrics for each pair of objects to be packaged: the KS aggregated distances between all the triangular facet pairs and the length of the intersection curve(s) between the two objects (if any). When adequately constrained in the optimization, these metrics produce spatially-feasible packing solutions.

[†]`https://github.com/mdolab/mach-aero`

There is a tuning parameter, ρ in the KS function, which controls how conservative the constraint aggregator is. Choosing a larger ρ gives a more exact result for the constraint, but it increases the constraint curvature. Excessively-large ρ will prevent the optimizer from taking efficient steps near the active zone due to the aggressive curvature. Unless otherwise specified, we used $\rho = 250$ for all the described cases below.

The Tensorflow implementation in the previous work was well-suited to a desktop environment with a GPU; however, its CPU runtime was not scaling well. The new Fortran implementation enables orders of magnitude speedup via heuristics such as bounding-box testing. We compute derivatives of the outputs with respect to surface mesh inputs using the Tapenade automatic differentiation tool [20]. We wrapped the Fortran codebase in Python using the f2py utility [21].

C. Optimization

To solve the MDO problem, we use the gradient-based nonlinear optimizer SNOPT 7.7.5 [22, 23]. We wrap SNOPT using the Python interface pyOptSparse [24]. We exploit a unique feature of SNOPT in this problem. In our experience, optimizers often take steps that are too big early on in a packing problem, before a good quasi-Newton estimate of the constraint curvature is built up in the optimizer. To prevent unreasonably large steps from consuming wall time, we pass a "fail" flag to SNOPT if any packing objects intersect by more than a moderate tolerance during a step. When this happens, we also prevent the aerostructural solution or adjoints from running. SNOPT then backtracks by a factor of ten and continues. Significant time savings can be achieved this way.

Because we are using constraint aggregation for both the structural failure constraints and spatial integration, the optimization problems have aggressive curvature near the optimum. This is a challenging scenario for the optimizer. The optimizer computes an internal optimality criterion, and it usually expects this figure to drop by six orders of magnitude for successful convergence. We find qualitatively that the optimality metric stays artificially high when constraint aggregation is used, preventing the optimizer from a “normal” exit. Our criteria for run convergence in this paper include:

- Optimality metric on the order of 10^{-3} or less
- Feasibility metric on the order of 10^{-4} or less
- Diminished continued improvement (per-iteration improvement on the order of 0.01%)

We ran the cases using two or three Intel Skylake nodes on the Stampede2 supercomputer at the University of Texas—a total of 96 to 144 physical processors.

V. Results

This section contains a progression of optimization results for the wing-tank problem with increasing complexity. First, we kept the wingbox fixed and optimized the tank shape only for maximum volume. Next, we allowed the wing outer mold line to vary, but considered only packing and aerodynamics, and minimized drag subject to a fuel volume constraint. Then, we ran a series of aerostructural optimization cases with all design variables active.

A. Optimizing Tank Shape Only

As a simple test, we exercised the CAD-based tank geometry by maximizing the volume of the tanks V_{tank} within the baseline wing box. Since there was no high-fidelity analysis in the loop, we used a Linux desktop for this case. Because there were fewer design variables and constraints, we chose a slightly more aggressive $\rho = 300$. We found that the maximum achievable volume was approximately 1.718 m^3 and the optimizer converged without difficulty. Table 1 lists the design variables, objective, and constraints and Figure 6 illustrates the resulting geometry (in black). The tanks expand to efficiently fill the wingbox, as expected.

		Quantity	Lower	Upper	Scaling
maximize	V_{tank}	1			1.0
with respect to	Tank radius	7	0.14 m	3.0 m	0.1
	Tank length	7	1.0 m	2.5 m	0.1
	Tank x-y offset	14	−0.2 m	0.2 m	0.1
	Tank tilt	7	−1.0 °	4.0 °	1.0
	Total number of design variables	**35**			
subject to	Packing (aggregated distance)	7	0.0 m		100
	Intersection perimeter	7		0.0 m	1.0
	Total number of constraints	**14**			

Table 1 Problem formulation: tank shape optimization for maximum volume

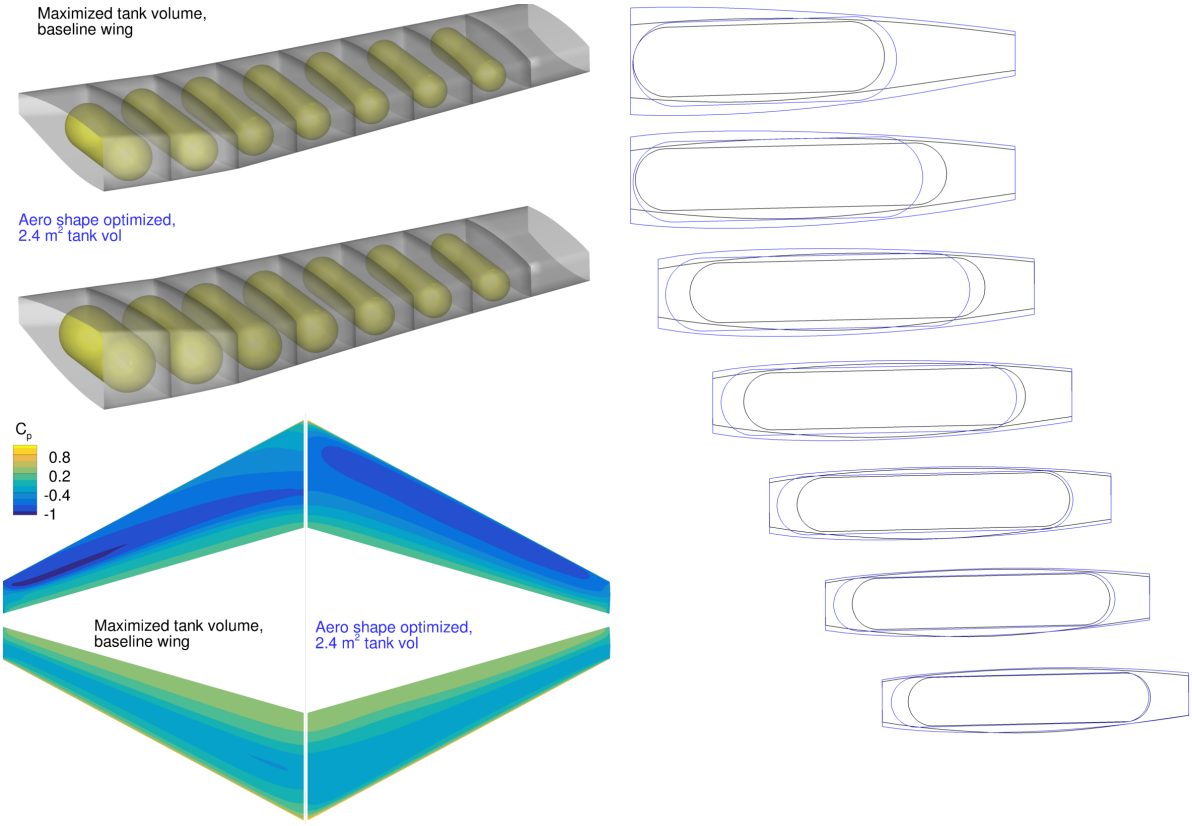

Fig. 6 Solutions to the volume maximization and minimum drag subproblems

B. Optimizing Wing OML and Tank Shape

Next, we increased the degree of difficulty substantially by adding aerodynamic physics. We add the angle of attack and outer mold line shape variables to the problem and include a constraint balancing lift L and weight W (a notional cruise condition). Because they have entirely separate geometric parameterizations, the inner tanks and OML are only coupled via the spatial integration constraints. The objective is to minimize drag D subject to a minimum hydrogen fuel volume constraint of 2.4 m^3 (arbitrary, but intended to push out the OML a reasonable amount). The KS parameter ρ remains at 300 for comparison to the volume-only case. The problem summary is in Table 2 and the optimization result is included in Figure 6 (in blue). We see that the inboard OML grows substantially to accommodate larger diameter tanks. The optimizer strategically adds thickness near the aft spar to allow tanks to expand rearward. The far outer part of the wing is constrained by minimum thickness.

		Quantity	Lower	Upper	Scaling
minimize	D	1			1.0
with respect to	Angle of attack	1	0 °	10 °	0.1
	Sectional shape	96	−0.5	0.5	1.0
	Tank radius	7	0.14 m	3.0 m	0.1
	Tank length	7	1.0 m	2.5 m	0.1
	Tank x-y offset	14	−0.2 m	0.2 m	0.1
	Tank tilt	7	−1.0 °	4.0 °	1.0
	Total number of design variables	**132**			
subject to	$L - W$ (cruise)	1	0 N	0 N	$1/W$
	V_{tank}	1	2.4 m^3		1.0
	Wingbox thickness (vs. baseline)	100	1.0		1.0
	Packing (aggregated distance)	7	0.0 m		100
	Intersection perimeter	7		0.0 m	1.0
	Total number of constraints	**116**			

Table 2 Problem formulation: aerodynamic shape optimization of wing and fuel tanks for minimum drag

C. Aerostructural Optimization at Fixed Tank Volume

This case adds structural analysis, including a 2.5 g maneuver condition (Figure 8), and structural design variables to the previous problem. In the absence of a whole-airplane performance model, this aerostructural optimization is a multiobjective problem between wing weight and drag. We simply choose $2W_{\text{wing, struct}} + D$ as a reasonable compromise objective function. Table 3 describes the problem formulation.

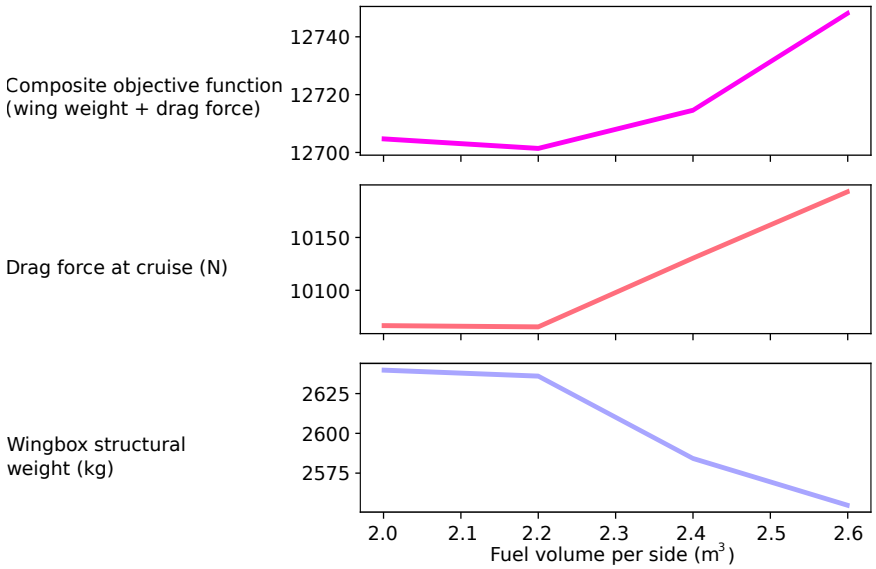

Fig. 7 Increasing fuel storage in the wing requires an aerostructural penalty, though aerodynamics and structure move in opposite directions

Consider an aircraft design team that wishes to know how adding fuel volume in the wing might affect weight and aerodynamic performance. This is an important piece of information when deciding how to allocate fuel throughout the whole airplane. We can answer this problem using packing optimization. We ran the problem in Table 3 at several fuel volume requirements, from 2.0 to 2.6 m^3. Figure 7 shows how the aerostructural performance of the airplane changes as fuel volume is added. At 2.2 m^3 or less, the wing aerostructural optimum has enough room to accommodate the tanks

without affecting the design. At 2.4 m^3 tank volume and above, the optimizer can no longer accommodate the tanks without pushing out the OML, incurring a sharp rise in drag. The drag increase is partially offset by a structural weight *decrease* due to the increased structural depth at the side-of-body.

This example illustrates why it is essential to consider multiple disciplines when evaluating spatial integration tradeoffs. Without optimization, engineers would need to perform laborious analysis and iterate internally to achieve a good result. Using our optimization framework, each of the runs used 400 to 600 core-hours on the HPC (four to six hours wall time each). If the cases run in parallel on an in-house or cloud HPC service, it is easily conceivable that the data for this trade study could be collected and analyzed in one working day.

Figure 9 illustrates the solution for 2.4 m^3 fuel volume (in black).

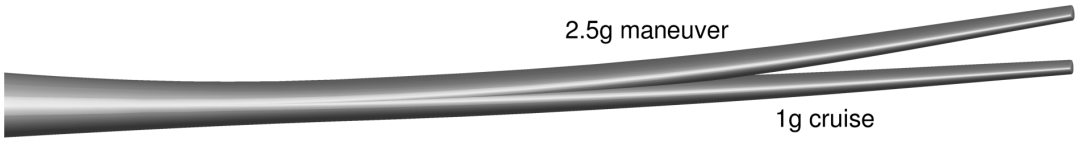

Fig. 8 Aeroelastic solutions at the cruise and maneuver conditions

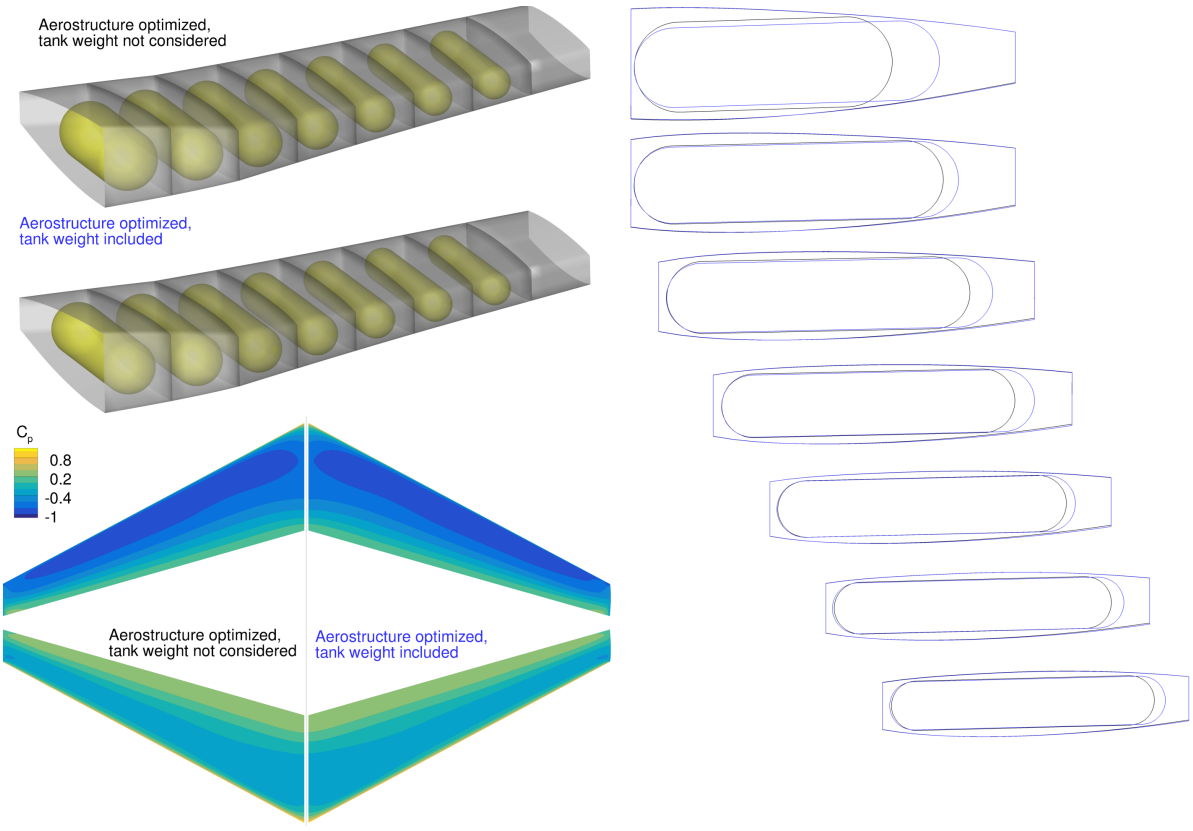

Fig. 9 Solutions to the aerostructural problem with and without considering the weight of the tanks

		Quantity	Lower	Upper	Scaling
minimize	$2W_{\text{wing, struct}} + D$	1			1.0
with respect to	Angle of attack	2	0 °	10 °	0.1
	Stringer thickness	54	0.0016 m	0.02 m	100.0
	Spar thickness	18	0.0016 m	0.02 m	100.0
	Skin thickness	18	0.0016 m	0.02 m	100.0
	Rib thickness	18	0.0016 m	0.02 m	100.0
	Sectional shape	96	−0.5	0.5	1.0
	Tank radius	7	0.14 m	3.0 m	0.1
	Tank length	7	1.0 m	2.5 m	0.1
	Tank x-y offset	14	−0.2 m	0.2 m	0.1
	Tank tilt	7	−1.0 °	4.0 °	1.0
	Total number of design variables	**241**			
subject to	$L - W$ (cruise)	1	0 N	0 N	$1/W$
	$L - 2.5W$ (maneuver)	1	0 N	0 N	$1/W$
	V_{tank}	1	various m^3		1.0
	Structural failure at 2.5 g (aggregated)	3		1.0	1.0
	Wingbox thickness (vs. baseline)	100	1.0		1.0
	Packing (aggregated distance)	7	0.0 m		100
	Intersection perimeter	7		0.0 m	1.0
	Total number of constraints	**120**			

Table 3 Problem formulation: aerostructural design optimization of wing and fuel tanks with composite objective

D. Aerostructural Optimization Considering Tank Weight

While the previous subsections showed a series of successful aerostructural optimization packing cases, we have still neglected a significant effect: hydrogen tank weight. Because of the extreme pressure and low density of the compressed fuel, even a CFRP composite tank will have a hydrogen fuel fraction significantly less than ten percent [25]. The radius and length of the tank will affect its weight significantly.

Offline, we set up a structural optimization problem to minimize the weight of a tank made from a bidirectional carbon fiber laminate, considering both axial and hoop stresses [‡]. The method uses a simplified classical laminate theory model and computes the required laminate thickness in the cylindrical portion of the tank subject to hoop and axial stress. We compared the optimization model to a detailed finite element study of a CFRP tank [25] and found that our structural weight estimate was within 15% of the published value [§]. At 700 bar and 2.35 burst pressure safety factor, using an optimal bidirectional laminate with Toray 1100G prepreg [26], we found that the optimal tank wall thickness is a constant 0.1315 times the tank radius. Therefore, we did not need to explicitly incorporate tank structural analysis into the optimization—only a weight calculation based on tank radius and length. The density of the CFRP material is 1,573 kg/m^3. The problem formulation is summarized in Table 4.

The resulting geometry is visualized in Figure 9 (in blue). While the OML only changes subtly at the lower trailing edge, the changes allow the tanks to become much longer and narrower, reducing hoop stress and tank weight. This is a complex tradeoff between the structural weight of a component and the structural weight and drag at the airplane level. It is a good illustration of MDO's potential to find non-obvious solutions in airplane trade studies rapidly.

Figure 10 shows the structural sizing variables for this case. Some of the structural zones are minimum gauged, such as the ribs and some spar web zones. Figure 11 shows the structural failure criterion at the 2.5 g maneuver case. We can see that the optimizer has removed material almost everywhere until most of the wingbox is nearly at failure at ultimate load (2.5 g plus 1.5 safety factor).

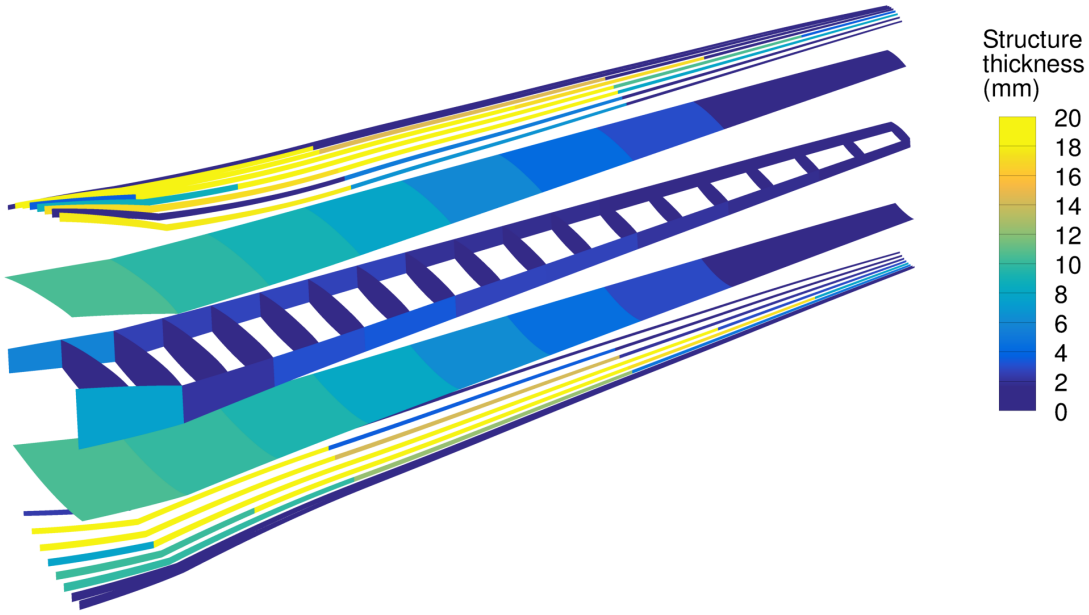

Fig. 10 Structural sizing variables at the optimum (with tank weight, 2.4 m^3 fuel volume)

[‡] https://gist.github.com/bbrelje/b599102f2d83749df681dd5c2c0865e1
[§] https://gist.github.com/bbrelje/947ef6ff401a201812fde465518b74ff

		Quantity	Lower	Upper	Scaling
minimize	$2(W_{\text{wing, struct}} + W_{\text{tanks}}) + D$	1			1.0
with respect to	Angle of attack	2	0 °	10 °	0.1
	Stringer thickness	54	0.0016 m	0.02 m	100.0
	Spar thickness	18	0.0016 m	0.02 m	100.0
	Skin thickness	18	0.0016 m	0.02 m	100.0
	Rib thickness	18	0.0016 m	0.02 m	100.0
	Sectional shape	96	-0.5	0.5	1.0
	Tank radius	7	0.14 m	3.0 m	0.1
	Tank length	7	1.0 m	2.5 m	0.1
	Tank x-y offset	14	-0.2 m	0.2 m	0.1
	Tank tilt	7	-1.0 °	4.0 °	1.0
	Total number of design variables	**241**			
subject to	$L - W$ (cruise)	1	0 N	0 N	$1/W$
	$L - 2.5W$ (maneuver)	1	0 N	0 N	$1/W$
	V_{tank}	1	2.4 m^3		1.0
	Structural failure at 2.5 g (aggregated)	3		1.0	1.0
	Wingbox thickness (vs. baseline)	100	1.0		1.0
	Packing (aggregated distance)	7	0.0 m		100
	Intersection perimeter	7		0.0 m	1.0
	Total number of constraints	**120**			

Table 4 Problem formulation: aerostructural design optimization of wing and fuel tanks with composite objective, considering tank weight

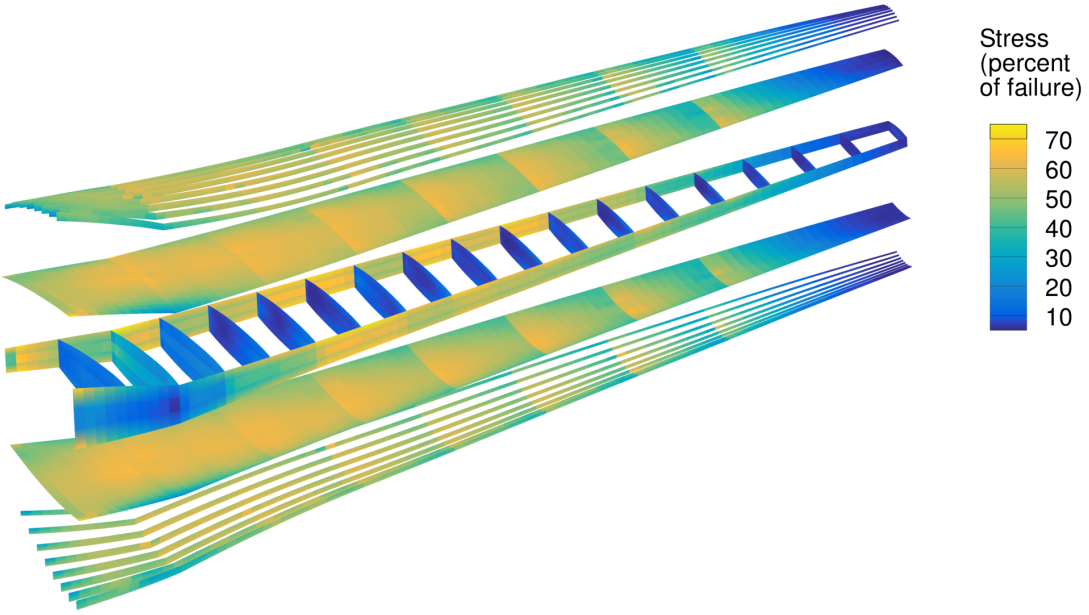

Fig. 11 Structural failure criterion at the optimum (with tank weight, 2.4 m^3 fuel volume)

E. Aerostructural Optimization for Maximum Range

In the previous example, we relied on a composite objective function in the absence of an airplane-level performance model and assumed a given fuel volume. We can make some assumptions and gain some intuition on whether placing compressed hydrogen in the wing of this test case airplane is viable. For the new objective function, let us maximize the range subject to a design payload.

Since we don't have an airplane-level empty weight model, we assume that the aircraft's operating empty weight (OEW) is 53% of MTOW and that the design payload is 23% of MTOW. We subtract the wing structure's weight from the previous optimum point (2,586 kg) and obtain OEW-less-wing of 26,511 kg. We then attribute the remaining 24% weight to fuel. A small fraction of the fuel is wing fuel from the previous optimum point (100.8 kg hydrogen at 42 kg/m^3 plus 1070.7 kg tank weight per wing). The remainder is computed at 9% hydrogen weight fraction and installed in the fuselage (975 kg hydrogen plus 9858 kg tank weight).

The actual TOW can now be computed as:

$$W_{\text{TO}} = W_{\text{payload}} + \text{OEW}_{\text{less wing}} + W_{\text{fuselage fuel}} + W_{\text{fuselage tank}} + 2(W_{\text{wing structure}} + W_{\text{wing tank}} + W_{\text{wing fuel}}) \tag{1}$$

and the zero fuel weight as:

$$W_{\text{zero fuel}} = W_{\text{payload}} + \text{OEW}_{\text{less wing}} + W_{\text{fuselage tank}} + 2(W_{\text{wing structure}} + W_{\text{wing tank}}) \tag{2}$$

An obvious limitation of this simplified model is that it neglects OEW growth outside the wing due to MTOW growth.

Now that we have pre- and post-mission weights, we can compute the range using the Breguet range equation as follows:

$$R = \frac{U_\infty}{g}\frac{L}{D}\frac{1}{1000\,\text{SFC}} ln \frac{W_{\text{TO}}}{W_{\text{zero fuel}}} \tag{3}$$

where R is the range in km, g is the gravitational constant, U_∞ is the true airspeed in m/s, SFC is the specific fuel consumption in kg/Ns (assumed to be 1.5×10^{-5}, slightly better than published figures for previous-generation single aisle turbofans). We can correct this SFC to account for the higher heating value of hydrogen compared to kerosene (nearly three times greater), but it won't affect the optimization result. With the heat value correction, the previous optimum airplane is computed to have a range of about 1900 km at design payload—much less than contemporary single aisles, but much more than all-electric proposals. We can now optimize the airplane with respect to this objective function as described in Table 5.

		Quantity	Lower	Upper	Scaling
maximize	range (km)	1			0.001
with respect to	Angle of attack	2	0 °	10 °	0.1
	Stringer thickness	54	0.0016 m	0.02 m	100.0
	Spar thickness	18	0.0016 m	0.02 m	100.0
	Skin thickness	18	0.0016 m	0.02 m	100.0
	Rib thickness	18	0.0016 m	0.02 m	100.0
	Sectional shape	96	-0.5	0.5	1.0
	Tank radius	7	0.14 m	3.0 m	0.1
	Tank length	7	1.0 m	2.5 m	0.1
	Tank x-y offset	14	-0.2 m	0.2 m	0.1
	Tank tilt	7	-1.0 °	4.0 °	1.0
	Total number of design variables	**241**			
subject to	$L - W$ (cruise)	1	0 N	0 N	$1/W$
	$L - 2.5W$ (maneuver)	1	0 N	0 N	$1/W$
	Structural failure at 2.5 g (aggregated)	3		1.0	1.0
	Wingbox thickness (vs. baseline)	100	1.0		1.0
	Packing (aggregated distance)	7	0.0 m		100
	Intersection perimeter	7		0.0 m	1.0
	Total number of constraints	**119**			

Table 5 Problem formulation: aerostructural design optimization of wing and fuel tanks for maximum range

Figures 12 and 13 illustrate that, for this demonstration airplane, it is favorable to add more fuel tank volume in the wing root, even after considering the aerodynamic, structural, and weight penalties using high-fidelity physics. The optimizer increased each wing's fuel volume from 2.4 to 3.1 m^3.

This is a technology validation study for the optimization approach, not an airplane study per se. Our CFD and structural meshes were reasonably coarse, and the airplane-level weight model was of very low fidelity. We were not explicitly modeling the fuel cell or electric propulsion system. Nonetheless, the result suggests that storing compressed hydrogen in the wing root of a transport-class airplane can, in principle, be favorable even after considering aerodynamic and structural penalties. While this result cannot and should not be generalized to other configurations, it illustrates that compressed hydrogen may be an intriguing fuel for regional-length missions.

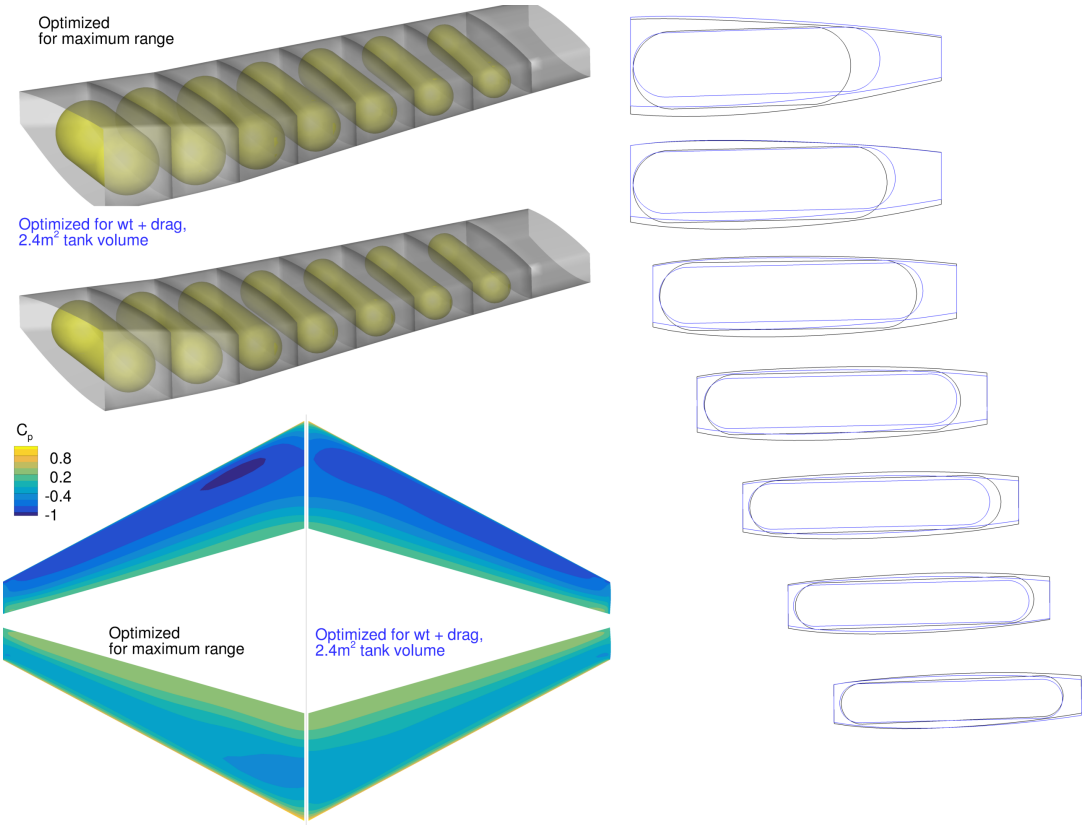

Fig. 12 The maximum range optimization problem adds significant fuel volume and root thickness

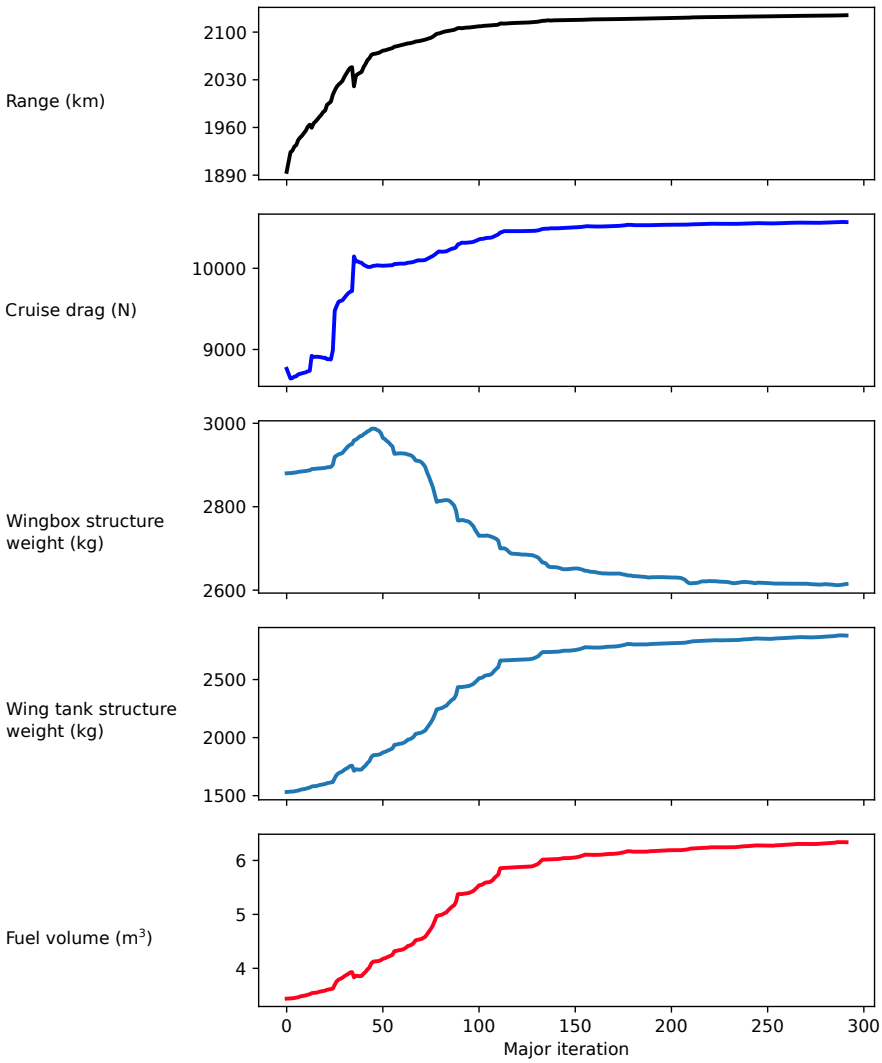

Fig. 13 The optimizer increases range at the expense of tank weight and drag by adding fuel volume

VI. Conclusion

Hydrogen fuel is an intriguing option for zero-emissions aviation at typical commercial transport ranges. However, its extremely low density and inadequate options for mitigating this fact (high pressure or deep cryogenics) create spatial integration challenges for airplane designers (and thus providing a relevant test case for our technical approach to multidisciplinary packing problems). By solving a series of aerostructural packing optimization problems involving a wing and several hydrogen fuel tanks, we have validated the approach on a problem of significantly greater complexity than previously demonstrated. We showed that MDO can be used to perform spatial integration trade studies on a relevant wing design using high-fidelity aerostructural physics and the new KS-distance geometry constraint. We find that the aerostructural packing optimization runs can be performed on relevant time scales (less than one eight-hour shift using modest HPC resources). The optimization runs converge with regularity and identify subtle changes in OML shape that enable major improvements in system capability.

Despite the limitations we acknowledge above, our results suggest that storing compressed hydrogen in the wing root of a single-aisle transport *may* be a useful option at the airplane level. Compressed hydrogen may be feasible for regional-length missions outside the reach of battery-electric airplanes. However, the immense weight of compressed hydrogen storage, even under the relatively optimistic weight assumptions we make here, is a significant drawback of the compressed hydrogen approach and probably forecloses the possibility of using it for transcontinental routes. Other potential zero-carbon fuels (such as ammonia) should be explored in parallel.

Acknowledgments

The first author was supported by the National Science Foundation Graduate Research Fellowship Program under Grant DGE 1256260. Any opinions, findings, and conclusions or recommendations expressed in this material are those of the author(s) and do not necessarily reflect the views of the National Science Foundation. This work was also supported by the U.S. Air Force Research Laboratory (AFRL) under the Michigan–AFRL Collaborative Center in Aerospace Vehicle Design (CCAVD), with Dr. Richard Snyder as the task Technical Monitor. The authors acknowledge the Texas Advanced Computing Center (TACC) at The University of Texas at Austin for providing HPC resources that have contributed to the research results reported within this paper.

References

[1] Brelje, B., and Martins, J. R. R. A., "Electric, Hybrid, and Turboelectric Fixed-Wing Aircraft: A Review of Concepts, Models, and Design Approaches," *Progress in Aerospace Sciences*, Vol. 104, 2019, pp. 1–19. doi:10.1016/j.paerosci.2018.06.004.

[2] Lapeña-Rey, N., Mosquera, J., Bataller, E., and Ortí, F., "First Fuel-Cell Manned Aircraft," *Journal of Aircraft*, Vol. 47, No. 6, 2010, pp. 1825–1835. doi:10.2514/1.42234.

[3] Kramer, D., "Hydrogen-powered aircraft may be getting a lift," *Physics Today*, Vol. 73, No. 12, 2020, pp. 27–29. doi:10.1063/PT.3.4632.

[4] Silverstein, A., and Hall, E. W., "Liquid hydrogen as a jet fuel for high-altitude aircraft," Tech. Rep. RM E55C28a, NACA, Washington, DC, April 1955.

[5] Sloop, J. L., "Liquid hydrogen as a propulsion fuel, 1945-1959." Tech. Rep. SP 4404, NASA, Washington, DC, 1978.

[6] H2FLY, "The future of aviation," , 2020. URL `http://h2fly.de`.

[7] Brelje, B. J., Anibal, J., Yildirim, A., Mader, C. A., and Martins, J. R. R. A., "Flexible Formulation of Spatial Integration Constraints in Aerodynamic Shape Optimization," *AIAA Journal*, Vol. 58, No. 6, 2020, pp. 2571–2580. doi:10.2514/1.J058366.

[8] Brelje, B. J., and Martins, J. R. R. A., "Coupled component sizing and aerodynamic shape optimization via geometric constraints," *AIAA AVIATION Forum*, American Institute of Aeronautics and Astronautics, Dallas, TX, 2019. doi:10.2514/6.2019-3105.

[9] Kenway, G. K. W., and Martins, J. R. R. A., "Multipoint High-Fidelity Aerostructural Optimization of a Transport Aircraft Configuration," *Journal of Aircraft*, Vol. 51, No. 1, 2014, pp. 144–160. doi:10.2514/1.C032150.

[10] Kenway, G. K. W., Kennedy, G. J., and Martins, J. R. R. A., "Scalable Parallel Approach for High-Fidelity Steady-State Aeroelastic Analysis and Derivative Computations," *AIAA Journal*, Vol. 52, No. 5, 2014, pp. 935–951. doi:10.2514/1.J052255.

[11] Mader, C. A., Kenway, G. K. W., Yildirim, A., and Martins, J. R. R. A., "ADflow—An open-source computational fluid dynamics solver for aerodynamic and multidisciplinary optimization," *Journal of Aerospace Information Systems*, 2020. doi:10.2514/1.I010796.

[12] Yildirim, A., Kenway, G. K. W., Mader, C. A., and Martins, J. R. R. A., "A Jacobian-free approximate Newton–Krylov startup strategy for RANS simulations," *Journal of Computational Physics*, Vol. 397, 2019, p. 108741. doi:10.1016/j.jcp.2019.06.018.

[13] Secco, N. R., Jasa, J. P., Kenway, G. K. W., and Martins, J. R. R. A., "Component-based Geometry Manipulation for Aerodynamic Shape Optimization with Overset Meshes," *AIAA Journal*, Vol. 56, No. 9, 2018, pp. 3667–3679. doi:10.2514/1.J056550.

[14] Chan, W. M., and Steger, J. L., "Enhancements of a three-dimensional hyperbolic grid generation scheme," *Applied Mathematics and Computation*, Vol. 51, No. 2–3, 1992, pp. 181–205. doi:10.1016/0096-3003(92)90073-A.

[15] Kennedy, G. J., and Martins, J. R. R. A., "A Parallel Finite-Element Framework for Large-Scale Gradient-Based Design Optimization of High-Performance Structures," *Finite Elements in Analysis and Design*, Vol. 87, 2014, pp. 56–73. doi:10.1016/j.finel.2014.04.011.

[16] Sederberg, T. W., and Parry, S. R., "Free-form Deformation of Solid Geometric Models," *SIGGRAPH Comput. Graph.*, Vol. 20, No. 4, 1986, pp. 151–160. doi:10.1145/15886.15903.

[17] Kenway, G. K., Kennedy, G. J., and Martins, J. R. R. A., "A CAD-Free Approach to High-Fidelity Aerostructural Optimization," *Proceedings of the 13th AIAA/ISSMO Multidisciplinary Analysis Optimization Conference*, Fort Worth, TX, 2010. doi:10.2514/6.2010-9231.

[18] Luke, E., Collins, E., and Blades, E., "A Fast Mesh Deformation Method Using Explicit Interpolation," *Journal of Computational Physics*, Vol. 231, No. 2, 2012, pp. 586–601. doi:10.1016/j.jcp.2011.09.021.

[19] Haimes, R., and Dannenhoffer, J., "The Engineering Sketch Pad: A Solid-Modeling, Feature-Based, Web-Enabled System for Building Parametric Geometry," *21st AIAA Computational Fluid Dynamics Conference*, American Institute of Aeronautics and Astronautics, 2013. doi:10.2514/6.2013-3073.

[20] Hascoet, L., and Pascual, V., "The Tapenade automatic differentiation tool: Principles, model, and specification," *ACM Transactions on Mathematical Software*, Vol. 39, No. 3, 2013, pp. 20:1–20:43. doi:10.1145/2450153.2450158.

[21] Peterson, P., "F2PY: A tool for connecting Fortran and Python programs." *International Journal of Computational Science and Engineering*, Vol. 4, No. 4, 2009, pp. 296–305.

[22] Gill, P. E., Murray, W., and Saunders, M. A., "SNOPT: An SQP Algorithm for Large-Scale Constrained Optimization," *SIAM Review*, Vol. 47, No. 1, 2005, pp. 99–131. doi:10.1137/S0036144504446096.

[23] Gill, P. E., Murray, W., and Saunders, M. A., *User's Guide for SNOPT Version 7: Software for Large-Scale Nonlinear Programming*, Systems Optimization Laboratory, Stanford University, California, 94305-4023, 2007. Technical Report.

[24] Wu, N., Kenway, G., Mader, C. A., Jasa, J., and Martins, J. R. R. A., "pyOptSparse: A Python framework for large-scale constrained nonlinear optimization of sparse systems," *Journal of Open Source Software*, Vol. 5, No. 54, 2020, p. 2564. doi:10.21105/joss.02564.

[25] Hua, T. Q., Roh, H.-S., and Ahluwalia, R. K., "Performance assessment of 700-bar compressed hydrogen storage for light duty fuel cell vehicles," *International Journal of Hydrogen Energy*, Vol. 42, No. 40, 2017, pp. 25121 – 25129. doi:10.1016/j.ijhydene.2017.08.123.

[26] "Toray 3960 Prepreg System," Tech. rep., Toray Composite Materials America, 2020. URL `https://www.toraycma.com/files/library/0b1f847f1abb9142.pdf`.